Fabrication, Characterization, and Physical Analysis of AlGaN/GaN HEMTs on Flexible Substrates

N. Defrance, F. Lecourt, Y. Douvry, M. Lesecq, V. Hoel, A. Lecavelier Des Etangs-Levallois, Yvon Cordier, A. Ebongue, and J. C. De Jaeger

***Abstract*—This paper reports on the dc analysis and radio frequency (RF) characterization of a flexible AlGaN/GaN high-electron mobility transistor with a 120-nm gate length. The device provides a maximum dc current density of 470 mA/mm and a peak extrinsic transconductance of 125 mS/mm under flat condition. When the substrate is bent with 0.88% strain, a rise in the 2-DEG density is experimentally observed through the diminution of the on-resistance. This phenomenon is physically attributed to the modification of the piezoelectric field within the barrier under tensile condition. The device also shows a current gain cutoff frequency (F_t) of 32 GHz and a power gain cutoff frequency ($F_{\max}$) of 52 GHz. No major variations of RF performance are observed under bending.**

***Index Terms*—Electrical characterization, flexible substrate, GaN, high-electron mobility transistors (HEMTs), strain.**

I. Introduction

In RECENT years, transistors and circuits on flexible substrates have attracted a great deal of attention and open new opportunity for a wide range of applications such as flexible radio frequency (RF) identification tags, mobile sensors, flexible displays, etc.

The emerging applications require large bandwidth, high operating frequency, microwave power, and high efficiency performance. A way to obtain these characteristics consists to add conformability of plastic substrates to GaN-based devices whose capabilities were demonstrated for application in emission chains [1]. Indeed, at the present time, AlGaN/GaN high-electron mobility transistors (HEMTs) exhibit very high performance owing to improvements in both epimaterial and processing [2]. New opportunities in terms of high performance, low cost, and lightweight circuit design can be brought based on a rather simple transfer of these components onto a flexible substrate.

Manuscript received February 20, 2012; revised November 13, 2012; accepted January 4, 2013. Date of publication February 1, 2013; date of current version February 20, 2013. The review of this paper was arranged by Editor S. Bandyopadhyay.

N. Defrance, F. Lecourt, Y. Douvry, M. Lesecq, V. Hoel, A. Lecavelier Des Etangs-Levallois, and J. C. De Jaeger are with the Institute of Electronics, Microelectronics and Nanotechnologies (IEMN), Cité Scientifique, 59650 Villeneuve d'Ascq, France (e-mail: Nicolas.Defrance@iemn.univ-lille1.fr; francois.lecourt@ed.univ-lille1.fr; yannick.douvry@ed.univ-lille1.fr; marie.lesecq@iemn.univ-lille1.fr; Virginie.Hoel@IEMN.Univ-Lille1.fr; aurelien.lecavelier@isen.iemn.univ-lille1.fr; jean-claude.dejaeger@iemn.univ-lille1.fr).

Y. Cordier is with CNRS-Research Center for Heteroepitaxies and their Applications (CRHEA), 06560 Valbonne, France (e-mail: yc@crhea.cnrs.fr).

A. Ebongue is with 3M Company, 95250 Beauchamp, France (e-mail: aebongue@mmm.com).

Color versions of one or more of the figures in this paper are available online at http://ieeexplore.ieee.org.

Digital Object Identifier 10.1109/TED.2013.2238943

Lee *et al.* [3] proposed a first investigation regarding AlGaN/GaN HEMTs on a polyethylene terepthalate flexible substrate. Recently, we reported better high dc performance of AlGaN/GaN HEMTs on adhesive flexible tape [4]. In this paper, for the first time to our knowledge, the RF performance of GaN HEMTs on adhesive flexible tape is presented, showing that these new devices constitute an attractive way for future applications at high frequency when conformability is needed.

II. Transistor Fabrication

The transistor fabrication is based on three steps. In a first time, a molecular beam epitaxy is grown on a silicon [111] substrate. It consists of a 21-nm AlGaN barrier layer with an Al content of 28%, a 1-nm AlN exclusion layer, a 1.73-μm GaN channel, and AlN/GaN/AlN interlayers (250 nm/250 nm/42 nm) to mitigate stress in the active area. Hall effect measurements permit to extract a sheet carrier density of 8.7×10^{12} cm^{-2} and an associate electron mobility of 1780 cm$^2 \cdot$ V$^{-1} \cdot$ s^{-1}. The sheet resistance is thus evaluated to 403 Ω. Also, the transmission line model was used to extract the contact resistance, giving $R_c = 0.2(\pm 0.02)\Omega \cdot$ mm.

In a second time, devices are processed on a rigid Si substrate with conventional and stable fabrication steps using e-beam lithography described elsewhere for short gate length transistors [5]. In this paper, the gate length based on a three-resist-layer lithography process is $L_G = 120$ nm.

At last, the devices are transferred onto a flexible tape. The target flexible substrate is an adhesive flexible tape from 3M Company. It consists of a thermally enhanced copolymer carrier coated on one side with an acrylic adhesive. The transfer process is derived from the one reported in [6]. The front side of the components is temporarily bonded on an intermediate handling wafer using an optical resist interlayer. The silicon growth substrate is then completely removed using a mechanical lapping followed by a xenon difluoride etching. An AlGaN/GaN thin film with devices is finally released from the silicon substrate. The back side of the AlGaN/GaN thin film is then directly stuck on an adhesive flexible tape. At last, the handling wafer is debonded from components owing to the resist interlayer removal.

TLM measurement is also carried out after this transfer process. A contact resistance and a sheet resistance of $0.21\Omega \cdot$ mm and 402 Ω, respectively, are obtained. It must be mentioned that the sheet carrier density and the mobility are not accessible since the Hall effect apparatus is not usable with flexible

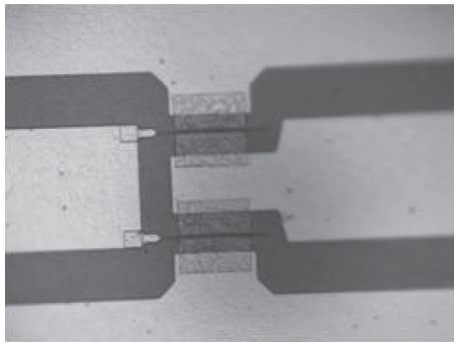

Fig. 1. Optical view of flexible device (Objective X 50).

substrates. Indeed, problems appeared with the probes involving damages in the transferred devices. Fig. 1 shows a microscope top view of a device supported on flexible tape.

III. Device Characterization

All dc and small-signal measurements are performed on $2 \times 50 \times 0.12$ μm^2 AlGaN/GaN HEMTs using microwave probes. The source-to-drain $(L_{\rm SD})$ and the gate-to-drain $(L_{\rm GD})$ spacing are 1.75 and 1.2 μm, respectively. Measurement is first performed on the device processed on the silicon substrate, i.e., before the Si[111] removal. The same measurements are then carried out on the devices after transfer on "flat" and "strained" conditions. This procedure permits to highlight both the effects of the transfer process and those of the strain on the electrical characteristics. Regarding under-strain characterization, the flexible substrate is bent on a semicylindrical base with a 15-mm radius of curvature corresponding to a 0.88% strain [7]. In this paper, the strain is induced in the gate width direction.

A. DC Characteristics

DC measurement is performed using an HP4142B static modular source and monitor. DC output $I_{\rm DS}$–$V_{\rm DS}$ characteristics are extracted for different values of $V_{\rm GS}$ and for different substrate conditions (silicon, flexible, and strained flexible). The effect of the transfer onto the flexible substrate, as well as the impact of a convex bending, is treated in the following paragraphs.

1) Effect of the Transfer on the DC Characteristics: A maximum drain current density $(I_{\rm DSMAX})$ of 930 mA/mm is obtained at $V_{\rm GS} = 0$ V before the transfer onto the 3M tape. This value severely drops down to 450 mA/mm once the device is transferred on the flexible tape (see Fig. 2). This decrease can be explained by the poor thermal conductivity of the polymer tape $(K_{\rm th} = 5 \times 10^{-3}\ {\rm W \cdot cm^{-1} \cdot K^{-1}})$, compared with $K_{\rm th}$(Si) which is about three orders of magnitude higher $(1.3\ {\rm W \cdot cm^{-1} \cdot K^{-1}})$. Nonetheless, it can be pointed out that the $I_{\rm DSMAX}$ value on the flexible tape is around 50% higher than those reported in a previous work for a transistor with a gate length of 2 μm [4].

To avoid any contribution of the thermal aspects in the analysis of the electrical behavior of this device, a study is

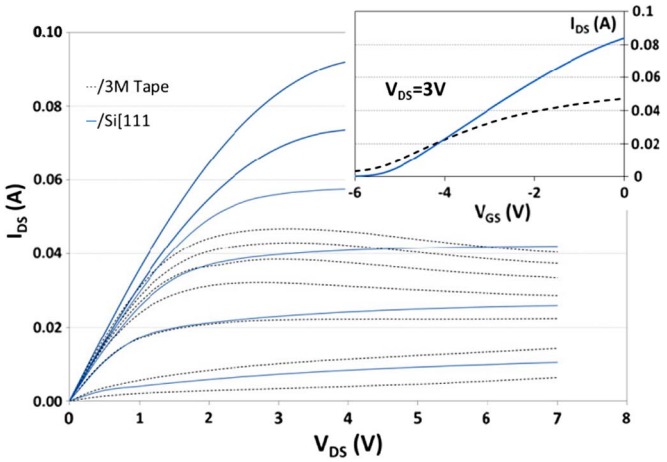

Fig. 2. $I_{\rm DS}$–$V_{\rm DS}$ characteristics of a $2 \times 50 \times 0.12$ μm^2 AlGaN/GaN HEMT measured before and after its transfer onto the flexible tape. $V_{\rm GS}$ sweeps from 0 V down to -5 V with a -1-V step.

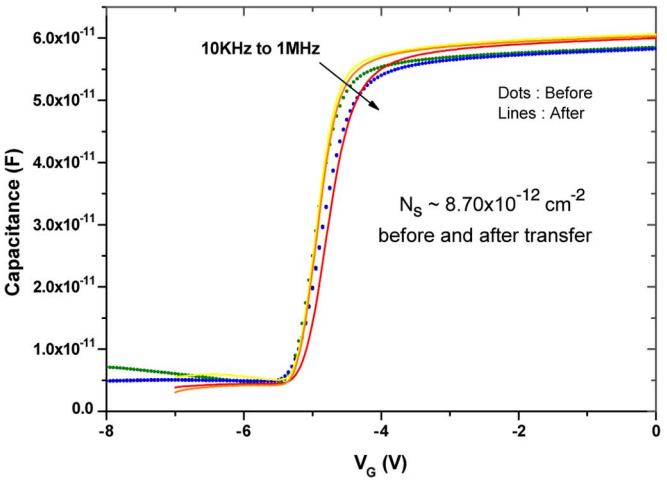

Fig. 3. C–V profiles of a 200×100 μm^2 pattern (dots) before and (lines) after the transfer. Measurement is carried out at 10 kHz, 100 kHz, and 1 MHz.

further carried out at very low drain bias ($V_{\rm DS} = 0.2$ V, i.e., within the linear part of the characteristics). This bias condition will be treated in the next section of this paper.

The transfer characteristics are also plotted in Fig. 3 for the same substrate conditions (i.e., HEMT on silicon, as well as once transferred). Regarding the HEMT on polymer, it can be noted that the $I_{\rm DS}$–$V_{\rm GS}$ curves above pinchoff do not follow the ideal linear evolution as the channel becomes more and more open [8]. This involves a notable decrease of the transconductance beyond its maximum value at $V_{\rm GS} = -4.8$ V. This tends to confirm the major impact of the bad thermal conductivity of the copolymer substrate compared with more traditional materials such as silicon.

To demonstrate the direct correlation between the decrease of the drain current and the thermal conductivity, capacitance–voltage profiles are shown in Fig. 4. The voltage sweeps between the pinchoff and the accumulation regime (i.e., from -8 to 0 V) while the frequencies (10 kHz, 100 kHz, and 1 MHz) are chosen to highlight possible traps and defects within the structure. The results are very interesting since no

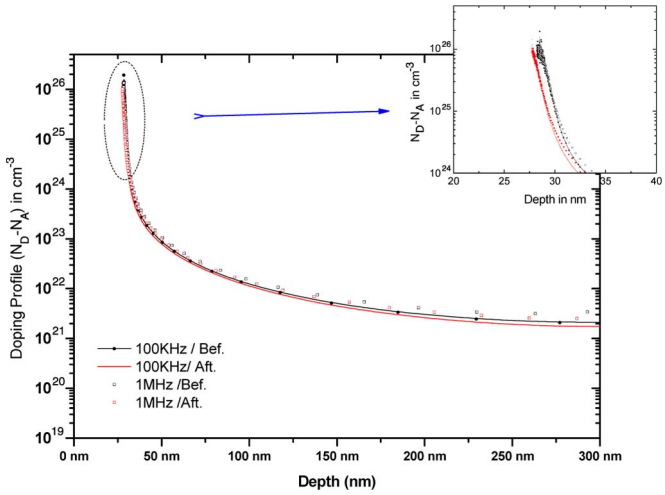

Fig. 4. Doping profiles of a 200×100 μm^2 pattern (black) before and (red) after transfer. The profiles are extracted from C–V characteristics measured at 100 kHz and 1 MHz.

deviation is observed either in terms of frequency dispersion or as regards charge density, which is obtained by

$$n_s = \int_{-\infty}^{+\infty} n(z)dz. \tag{1}$$

Integrating the C–V profiles at 1 MHz gives sheet densities of 8.70×10^{12} and 8.74×10^{12} cm^{-2}, respectively, before and after transfer, confirming the assumption that the observed $I_{\rm DS}$ decrease is solely linked to thermal aspects. By the way, this also indicates that the layer quality is preserved during the transfer process. From the C–V measurement, the doping profiles are also extracted from the expression [9]

$$N_D - N_A = \frac{C^3}{q\varepsilon_0\varepsilon}\frac{dV}{dC} \tag{2}$$

as function of the depth

$$z = \frac{\varepsilon_0\varepsilon}{C}.$$

This behavior is plotted in Fig. 4, where, as it was expected, the sheet density does not to decrease after the transfer. The 2-DEG confinement also remains the same since two orders of magnitude in the N_S concentrate within the first 5 nm of the GaN channel. At last, the buffer insulating properties are evaluated to 10^{-21} m^{-3} for the device before the silicon removal and after transfer onto the flexible tape.

All these results confirm the efficiency of the transfer process since the 2-DEG density is not affected. In the same way, the similarities in the frequency-dependent C–V profiles permit to assume that no additional defects are created during the process.

2) Effect of the Bending on the DC Characteristics: In this part, the dc characteristics are shown once the device is transferred onto the 3M tape, under "flat" and "bent" conditions. The bending is established by means of a semicylindrical chuck featuring a 15-mm radius of curvature. Strain is induced in the gate width direction.

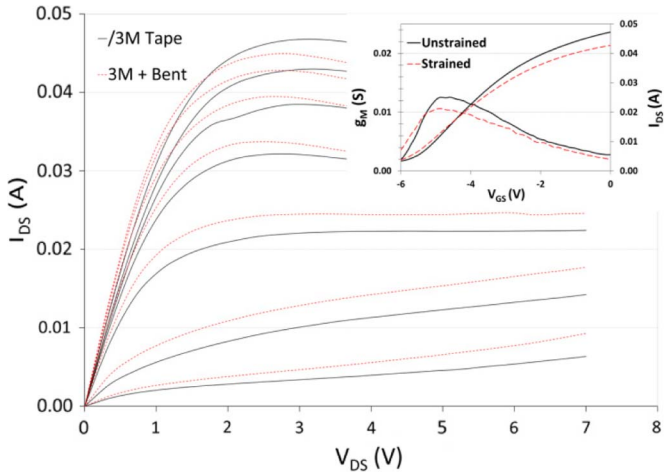

Fig. 5. $I_{\rm DS}$–$V_{\rm DS}$ characteristics of a $2 \times 50 \times 0.12$ μm^2 AlGaN/GaN HEMT on the flexible tape under flat and bent conditions. $V_{\rm GS}$ sweeps from 0 V down to -6 V with a -1-V step.

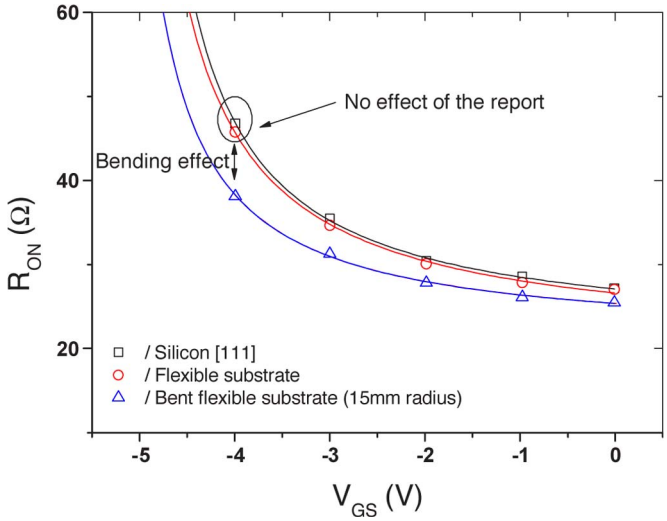

Fig. 6. $R_{\rm ON}$ resistance for a $2 \times 50 \times 0.12$ μm^2 HEMT before and after its transfer and in curved conditions. The lines correspond to the fit with Berroth's model.

Fig. 5 shows the forward I–V characteristics of the same device in both conditions and the associated transconductance at $V_{\rm DS} = 3$ V (see inset in Fig. 5).

To avoid any confusion in the physical analysis, taking origin from the differences of the chuck thermal conductivity (the flat one is aluminum while the semicylindrical one is Teflon PFA), the study concentrates on the electrical behavior at very low source-to-drain bias, i.e., $V_{\rm DS} = 0.2$ V. For each case, the total on-resistance ($R_{\rm ON} = V_{\rm DS}/I_{\rm DS}$) is extracted and plotted versus the gate voltage $V_{\rm GS}$ (see Fig. 6). This plot permits to get information about the efficiency of the 2-DEG control and the carrier sheet density N_S of the layer as well. In order to evaluate them, Berroth's model [10] is used to fit the experimental data.

In this model, the on-resistance is assumed to behave as $R_{\rm ON} \sim R_S + RD + K(1/V_{\rm GS})$, with R_S and R_D being the source and drain resistances, respectively, and $K(1/V_{\rm GS})$ being a function tending to zero when $V_{\rm GS}$ increases. Hence, the

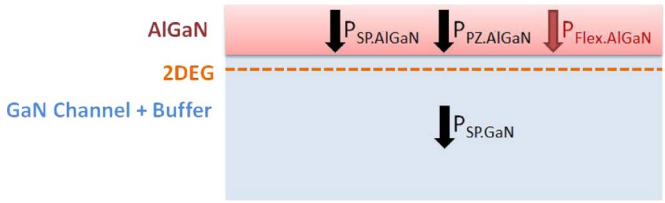

Fig. 7. Configuration of the polarization fields in the AlGaN/GaN structure considering the equilibrium and the curved conditions. At equilibrium, the GaN layer is assumed to be mechanically relaxed.

asymptotic value corresponds to $R_S + R_D$, which, in turn, gives information about the sheet resistance. In our case, values of 20.1 and 21.3 Ω are obtained for $R_S + R_D$ in the bent and flat conditions, respectively. It must be noticed that the transfer process does not have any impact on the on-resistance since the fits give identical values for all the parameters (including $R_S + R_D$). Hence, the difference in $R_S + R_D$ before and after bending can be expressed in terms of the sheet resistance variation from

$$\Delta(R_S + R_D) \sim \Delta R_S \times (L_{\rm GS} + L_{\rm GD})/W \tag{3}$$

with R_S being the sheet resistance, $L_{\rm GS}$ and $L_{\rm GD}$ being the source-to-gate and the gate-to-drain spacing, respectively, and W being the total gate width. Considering the design geometry ($L_{\rm GS} + L_{\rm GD} = 2.7\ \mu$m and $W = 100\ \mu$m), the sheet resistance decreases according to

$$R_S \sim 44\Omega \quad \text{thus} \quad \frac{\Delta R_s}{R_s} \sim 11\%.$$

In a first approximation, this diminution of the sheet resistance can be correlated to a corresponding increase of the 2-DEG density since $R_s = (qN_s\mu_n)^{-1}$. This correlation is analyzed in the next paragraph, wherein the impact of the bending on the piezoelectric polarization is investigated.

3) Physical Analysis: As III-N semiconductors are piezoelectric, any applied strain (either tensile or compressive) results in a modification of the induced surface charges. In our study, the 2-DEG density is deduced from the sum of all the polarization effects occurring within the heterostructure, following the equation

$$\sigma_s = (P_{\rm SP.GaN}) - (P_{\rm SP.AlGaN} + P_{\rm PZ.AlGaN}) \tag{4}$$

where $P_{SP.GaN}$ is the spontaneous piezoelectric contribution of the Ga-face oriented GaN buffer. Similarly, $P_{SP.AlGaN}$ and $P_{PZ.AlGaN}$ are the spontaneous and piezoelectric contributions of the AlGaN barrier layer. When the device is bent, additional piezoelectric field must be considered to extract the surface charge. In a convex configuration, the curvature results in an additive tensile stress which must be taken into account (see Fig. 7). The surface charge at the AlGaN/GaN interface becomes

$$\sigma_s = (P_{\rm SP.GaN} + P_{\rm Flex.GaN}) - (P_{\rm SP.AlGaN} + P_{\rm PZ.AlGaN} + P_{\rm Flex.AlGaN}).$$

The additional surface charge can thus be expressed as

$$|\Delta\sigma_S| = |P_{\rm Flex.GaN} - P_{\rm Flex.AlGaN}|. \tag{5}$$

The piezoelectric polarization magnitudes are

$$P_{\rm Flex} = e \times C^{-1} \times \sigma_{\rm Flex} \tag{6}$$

where $\mathbf{e}$, $\mathbf{C}$, and $\boldsymbol{\sigma}$ denote the piezoelectric constants, the elastic coefficients, and the induced elastic strain, respectively, within the materials. Considering a monoaxial deformation in random direction, we obtain

$$P_{\rm Flex} = [e_{31} \quad e_{31} \quad e_{33}] \times \begin{bmatrix} C_{11} & C_{12} & C_{13} \\ C_{12} & C_{11} & C_{13} \\ C_{13} & C_{13} & C_{33} \end{bmatrix}^{-1} \times \begin{bmatrix} \sigma_x \\ \sigma_y \\ 0 \end{bmatrix} \tag{7}$$

which, in turn, gives

$$P_{\rm Flex} = \frac{(\sigma_x + \sigma_y).\left(e_{31} - e_{33}\frac{C_{13}}{C_{33}}\right)}{(C_{11} + C_{12}) - \frac{2.C_{13}^2}{C_{33}}}. \tag{8}$$

In this last formula, the polarization magnitude can be extracted in each layer, considering that the strain $\sigma_x + \sigma_y = \sigma_{\rm Flex}$ is calculated according to the Stoney equation which has been adapted for different curvature radii in the x- and y-directions [11]. In the first order, it has been demonstrated that strain direction does not affect the induced piezoelectric polarization; hence, $\sigma_{\rm Flex}$ can be approximated to

$$\sigma_{\rm Flex.GaN} = \frac{E_{\rm GaN}h_{\rm GaN}^2}{6R} \tag{9a}$$

$$\sigma_{\rm Flex.AlGaN} = \frac{E_{\rm GaN}h_{\rm GaN}^2}{6R(1-\nu_S)h_{\rm AlGaN}} \tag{9b}$$

where $E_{\rm GaN}$ is the GaN Young modulus, $h_{\rm GaN}$ is the GaN thickness, R is the radius of curvature, v_s is the Poisson's ratio, and $h_{\rm AlGaN}$ is the barrier thickness. All the values used for the calculation are reported in Table I. It can be noticed that the AlGaN coefficient is linearly interpolated between AlN and GaN parameters considering the Al content in the barrier [12].

From all these values and calculations, it results in $P_{\rm Flex.AlGaN} = -8.2 \times 10^{-4}$ C · m^{-2}. The associated polarization in the GaN buffer appears negligible since it is four orders of magnitude lower ($\sim 3 \times 10^{-8}$ C · m^{-2}) than the calculated AlGaN contribution. It directly leads to

$$|\Delta\sigma_S| = 8.2 \times 10^{-4}\ \text{C.m}^{-2},$$

$$\text{thus} \quad |\Delta N_S| = \frac{|\Delta\sigma_S|}{q} \sim 5 \times 10^{11}\ \text{cm}^{-2}.$$

The variation of the 2-DEG density can be deduced before and after bending

$$\frac{|\Delta N_S|}{N_S} = \frac{5 \times 10^{11}}{8.7 \times 10^{12}} = 6\%.$$

TABLE I
GaN AND AlGaN PARAMETERS

	C_{11}	C_{12}	C_{13}	C_{33}	e_{31}	e_{33}
GaN	367	135	103	398	-0.49	0.73
$Al_{0.28}Ga_{0.72}N$	375	135.5	104.4	396	-0.52	0.93

	E_{GaN}	υ_S	h_{GaN}	h_{AlGaN}	R	
GaN	181	0.352	1.73µm	-	15mm	
$Al_{0.28}Ga_{0.72}N$	-	-	-	21nm	15mm	

An increase of 6% is thus expected as regards the 2-DEG density. This value can be compared with the 11% variation that was extracted from the RON measurement and modeling. Although the results do not yield truly identical values, the order of magnitude remains comparable. Furthermore, it is theoretically shown that the convex configuration benefits to the carrier density located at the AlGaN/GaN interface, as observed by the slight diminution of the sheet resistance observed in Section II. As a conclusion, it is demonstrated that the convex curvature increases the tensile strain within the barrier and, hence, the 2-DEG density. As a consequence, the sheet resistance decreases, and the on-resistance decreases as well.

B. RF Characteristics

In this paragraph, the RF characteristics of the device are studied in small-signal configuration. The effect of the bending on F_t and F_{MAX} magnitudes is presented.

The scattering parameters S_{ij} are measured from 0.25 to 40 GHz using an Agilent Technologies N5245A vector network analyzer and line-reflect-reflect-match calibration. Pad contributions are extracted measuring separately the gate (T_G) and the drain (T_D) access on dedicated patterns and through T-parameter formalism. The transfer parameters (and so the scattering parameters) at the device plane T_{Dev} can then be deduced from those directly measured at the probe plane T_{Meas} considering [13]

$$[T_{\mathrm{Dev}}] = [T_G]^{-1}[T_{\mathrm{Meas}}][T_D]^{-1}. \tag{10}$$

The following results are related to the characteristics obtained after such a de-embedding process.

Fig. 8 represents the current gain modulus $(|H_{21}|)$ and the Mason's maximum unilateral gain (U) deduced from S-parameter measurement versus the frequency. At $V_{\mathrm{DS}} = 3$ V and $V_{\mathrm{GS}} = -4.75$ V, an extrinsic current gain cutoff frequency (F_t) of 32 GHz is obtained whatever the strain condition showing the reliability of the technology. This value is comparable to the theoretical one, obtained through the equation $f_t = g_m/2\pi(C_{gs} + C_{gd})$, where g_m is the measured transconductance, C_{gs} is the gate-to-2DEG capacitance, and C_{gd} is the gate-to-drain feedback capacitance. Assuming $\varepsilon_{\mathrm{AlGaN}} = 8.3 \times 10^{-11}\ \mathrm{F \cdot m^{-1}}$ for a 28% aluminum content and in view of the topological values, a theoretical cutoff frequency f_t of 40 GHz is found. The difference between both results may be due to the approximations used to determine C_{gs} (and secondary C_{gd}). Indeed, in this case, only the metallurgic gate length is used rather than the effective gate length.

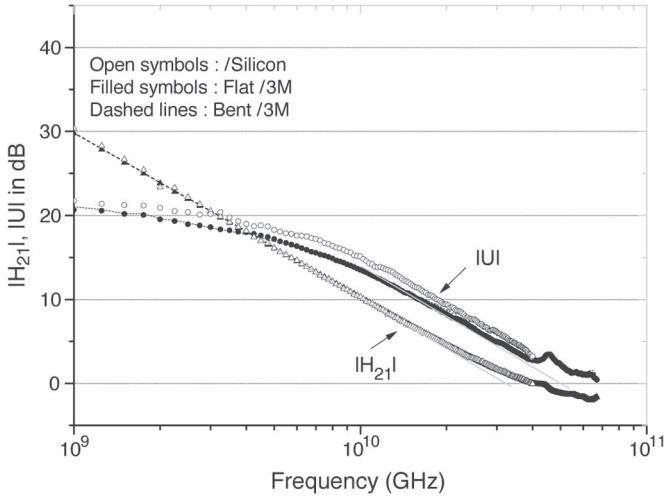

Fig. 8. Current gain and Mason's gain versus frequency for a $2 \times 50 \times 0.12\ \mu\mathrm{m}^2$ AlGaN/GaN HEMT on silicon and flexible substrate under flat and bent configurations.

Regarding the maximum power gain cutoff frequency (F_{max}) values, close to 52 GHz can be extracted before and during the bending. Therefore, attractive performance is demonstrated for AlGaN/GaN HEMTs on flexible substrate regarding microwave capabilities. It has to be noticed that both F_t and F_{max} values are very similar to those extracted before the transfer onto flexible substrate (i.e., 33 and 60 GHz, respectively). These agreements demonstrate the validity of the process since only a slight degradation is observed as regards small-signal performances.

IV. CONCLUSION

Flexible AlGaN/GaN HEMTs on flexible tape were fabricated. After transistor processing, the transfer is based on the silicon growth substrate removal followed by the simple bonding step on adhesive flexible tape.

It is shown that the flexible transistors withstand good dc power and demonstrate high RF performance with cutoff frequencies $F_t = 32$ GHz and $F_{\mathrm{max}} = 52$ GHz. Furthermore, the effect of the bending has been investigated experimentally and theoretically. A good quantitative agreement is observed between the RON reduction and the calculated 2-DEG density rise. Optimizing the flexible substrate thermal properties and dealing with reliability issues of GaN-on-flex technology might provide a promising way regarding new flexible circuits for future applications where medium power, high frequency, and flexibility are needed.

REFERENCES

[1] P. Schuh, R. Leberer, H. Sledzik, M. Oppermann, B. Adelseck, H. Brugger, R. Quay, M. Mikulla, and G. Weimann, "Advanced high power amplifier chain for X-band T/R-modules based on GaN MMICs," in *Proc. Eur. Microw. Integr. Circuits Conf.*, 2006, pp. 241–244.

[2] N. Baron, Y. Cordier, S. Chenot, P. Vennéguès, O. Tottereau, M. Leroux, F. Semond, and J. Massies, "The critical role of growth temperature on the structural and electrical properties of AlGaN/GaN high electron mobility transistor heterostructures grown on Si(111)," *J. Appl. Phys.*, vol. 105, no. 3, pp. 033701-1–033701-8, Feb. 2009.

[3] K. J. Lee, M. A. Meitl, J. H. Ahn, J. A. Rogers, R. G. Nuzzo, V. Kumar, and I. Adesida, "Bendable GaN high electron mobility transistors on plastic substrates," *J. Appl. Phys.*, vol. 100, no. 12, pp. 124507-1–124507-4, Dec. 2006.

[4] M. Lesecq, V. Hoel, A. Lecavelier Des Etangs-Levallois, E. Pichonat, Y. Douvry, and J. C. Dejaeger, "High performance of AlGaN/GaN HEMTs reported on adhesive flexible tape," *IEEE Electron Device Lett.*, vol. 32, no. 2, pp. 143–145, Feb. 2011.

[5] S. Bouzid, V. Hoel, N. Defrance, H. Maher, F. Lecourt, M. Renvoise, D. Smith, and J.-C. De Jaeger, "AlGaN/GaN HEMT on Si (111) substrate for millimeter microwave power applications," in *Proc. 8th Int. Conf. ASDAM*, Slomenice, Slovakia, Oct. 25–27, 2010, pp. 111–114.

[6] M. Lesecq, V. Hoel, A. Lecavelier, E. Pichonat, J. C. De Jaeger, Y. Douvry, F. Lecourt, A. Ebongue, and Y. Cordier, "AlGaN/GaN HEMTs reported on flexible polyimide substrate," in *Proc. 5th Space Agency- MOD Round Table Workshop GaN Compon. Technol.*, Noordwijk, The Netherlands, 2010, pp. 9–12.

[7] K. J. Lee, J. Lee, H. Hwang, Z. J. Reitmeir, R. F. Davis, J. A. Rogers, and R. G. Nuzzo, "A printable form of single-crystalline gallium nitride for flexible optoelectronic systems," *Small*, vol. 1, no. 12, pp. 1164–1168, Dec. 2005.

[8] Rashmi, A. Krantia, S. Haldarb, and R. S. Gupta, "An accurate charge control model for spontaneous and piezoelectric polarization dependent two-dimensional electron gas sheet charge density of lattice-mismatched AlGaN/GaN HEMTs," *Solid State Electron.*, vol. 46, no. 5, pp. 621–630, May 2002.

[9] D. K. Schroder, *Semiconductor Material and Device Characterization*, 3rd ed. Hoboken, NJ: Wiley, 2006, pp. 61–71.

[10] M. Berroth and R. Bosch, "Broad-band determination of the FET small-signal equivalent circuit," *IEEE Trans. Microw. Theory Tech.*, vol. 38, no. 7, pp. 891–895, Jul. 1990.

[11] N. Schwarzer and F. Richter, "On the determination of film stress from substrate bending: STONEY's formula and its limits," Chemnitz, Germany, 2006, Technical paper from University of Chemnitz, Biaxial tension in thin layers, Qucosa.

[12] Agilent Application Note 1364-1 De-embedding and Embedding S-Parameter Networks Using a Vector Network Analyzer, Agilent Application Note 1364-1.

[13] O. Ambacher, "Growth and applications of Group III-nitrides," *J. Phys. D, Appl. Phys.*, vol. 31, no. 20, pp. 2653–2710, Oct. 1998.

Authors' photographs and biographies not available at the time of publication.